

Accelerating Reaction Rates of Biomolecules by Using Shear Stress in Artificial Capillary Systems

Tuuli A. Hakala,[†] Emma V. Yates,[†] Pavan K. Challa, Zenon Toprakcioglu, Karthik Nadendla, Dijana Matak-Vinkovic, Christopher M. Dobson, Rodrigo Martínez, Francisco Corzana,^{*} Tuomas P. J. Knowles,^{*} and Gonçalo J. L. Bernardes^{*}



Cite This: *J. Am. Chem. Soc.* 2021, 143, 16401–16410



Read Online

ACCESS |



Metrics & More

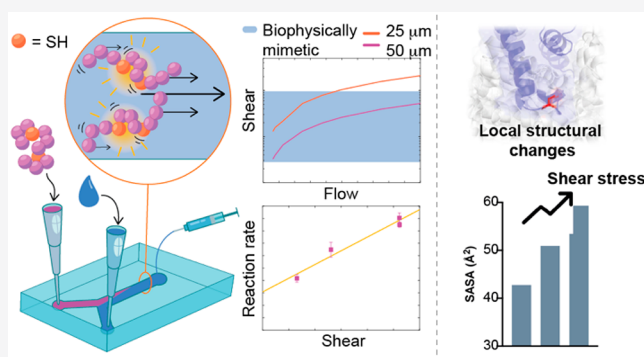


Article Recommendations



Supporting Information

ABSTRACT: Biomimetics is a design principle within chemistry, biology, and engineering, but chemistry biomimetic approaches have been generally limited to emulating nature's chemical toolkit while emulation of nature's physical toolkit has remained largely unexplored. To begin to explore this, we designed biophysically mimetic microfluidic reactors with characteristic length scales and shear stresses observed within capillaries. We modeled the effect of shear with molecular dynamics studies and showed that this induces specific normally buried residues to become solvent accessible. We then showed using kinetics experiments that rates of reaction of these specific residues in fact increase in a shear-dependent fashion. We applied our results in the creation of a new microfluidic approach for the multidimensional study of cysteine biomarkers. Finally, we used our approach to establish dissociation of the therapeutic antibody trastuzumab in a reducing environment. Our results have implications for the efficacy of existing therapeutic antibodies in blood plasma as well as suggesting in general that biophysically mimetic chemistry is exploited in biology and should be explored as a research area.



INTRODUCTION

Biomimetics, the emulation of nature's elements, models, and systems to solve human problems, is a key principle in many scientific fields including chemistry,¹ biology,² and engineering.³ Within chemistry, most biomimetic research to date has focused on exploiting nature's chemical toolkit.⁴ For example, biomimetic chemical reactions have allowed advances in the development biologically inspired synthetic transformation reactions, in the use of mild, aqueous reactions, as well as in the use of biological cofactors.^{5–9} However, within nature, biomolecules are subjected to distinct and variable conditions and forces which modulate their function. For example, biomolecules are frequently crowded or confined to small length scales, both of which can either promote or limit aggregation.^{10,11} Additionally, the elasticity of the extracellular matrix has been shown to control stem cell lineage specification.¹² Proteins within fibroblasts are subjected to contractile forces as the fibroblast pulls the cell body forward in a crawling motion through 3D tissue.¹³ As another example, shear stress within the circulatory system has been shown to alter the signaling pathways of endothelial cells via a mechanosensory complex,¹⁴ with higher shear stress generally associated with lower risk of atherosclerosis.¹⁵ Shear stress occurs when forces acting on a single body, such as a cell or a protein, pull it in different directions at the same time. Shear

stress has also been shown to promote post-translational modifications, specifically S-nitrosylation.¹⁶ Yet, redeployment of nature's physical architecture as a chemical tool remains largely unexplored.

We begin to explore the use of biophysically mimetic forces by considering shear stress experienced within capillaries. We consider this from both computational and experimental perspectives. A number of computational techniques which include Brownian dynamics and lattice-Boltzmann molecular dynamics (MD) have been developed to model the structural effect of shear stress on biomolecules.^{17–19} The methods were used to investigate flow-induced unfolding of a β -barrel protein in different types of flows²⁰ and stretching of integrin and ubiquitin.^{20–22} In a coarse-grained MD study, the unfolding of a β -hairpin, a WW domain, and a calcium-binding domain was reported.¹⁸ A similar coarse-grained approach was used to study the aggregation of several amyloidogenic peptides *in silico*.²³

Received: April 8, 2021

Published: October 4, 2021



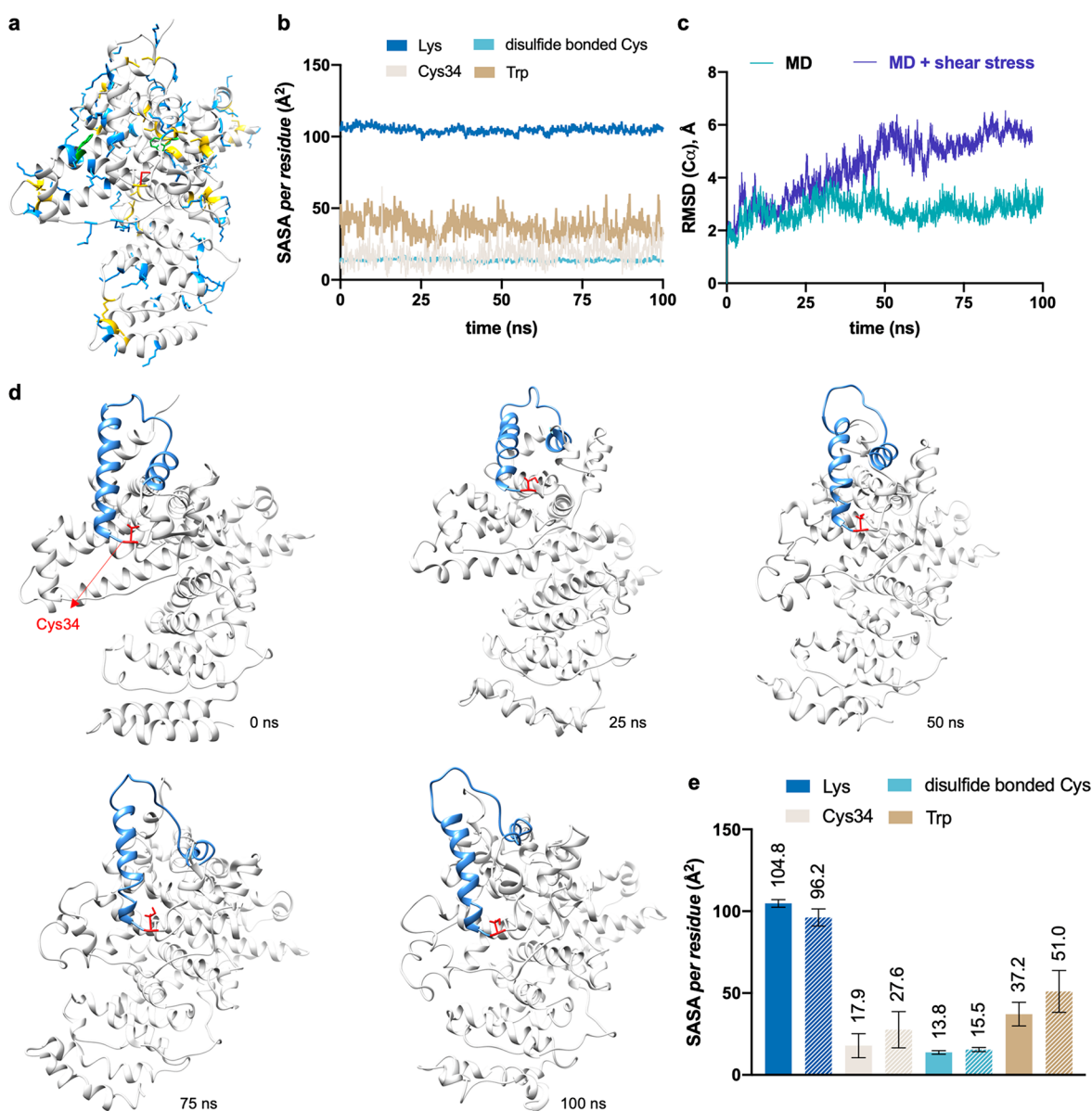


Figure 1. MD simulations of BSA in a shear flow. (a) Location of free Cys34 (in red), disulfide bonded Cys (in yellow), Lys (in blue), and Trp (in green) residues within BSA. (b) Average SASA along 100 ns conventional MD trajectory for these residues within BSA. (c) Evolution of root-mean-square displacement (RMSD) values of $C\alpha$ atoms of BSA along conventional MD and MD where the protein undergoes a shear flow (2.14×10^6 Pa). (d) Representative snapshots derived from 100 ns (MD simulations + shear flow) of BSA. (e) Average SASA values derived from 100 ns conventional trajectory (plain plot) or mimicking a shear flow (striped plot, shear stress 2.14×10^6 Pa) for free Cys34, disulfide bonded Cys, Lys, and Trp residues of BSA.

Here, we follow two different approaches to investigate the dynamics of biomolecules under these nonequilibrium conditions. In the first, proteins undergo a simple shear flow²⁴ that causes an increase in friction due to random collisions of the protein with nearby solvent or other solute molecules that exhibit rotational-translational diffusion. This computational approach has recently been applied to understand the rheo-NMR experiments performed on several proteins at the atomic level.²⁴ Alternatively, we perform steered MD simulations (SMD).^{25,26} In these calculations, we apply a force to two specific atoms that allows them to move from an initial position, given by the solved X-ray structure, to a position that we choose arbitrarily.^{27,28} In all calculations, one of the atoms chosen is the $C\alpha$ of the cysteine residue or the $C\alpha$ or a residue in close proximity to it (see the Supporting

Information for details). It is important to note that this external force does not represent a shear stress induced by the solvent and ion molecules. However, the two specified atoms were chosen to capture significant conformational changes around the cysteine residue through trajectories with a short time scale. Thus, this simple strategy allows us to mimic to a certain degree the deformation of the proteins subjected to shear flow. SMD simulations have been used to study amyloid fibril properties,²⁹ dissociation and association in response to shear,³⁰ the importance of hydrogen bonding in protein conformational locks,³¹ and protein unfolding,³² among others. The shear flow simulations and SMD simulations provide complementary views of the dynamics of biomolecules. In general, the application of both of these two computational approaches agree in showing marked increases in the solvent

accessible surface area (SASA) of certain residues, specifically free cysteine residues, rather than global protein unfolding.

We next study the impacts of this increase in SASA within a microfluidic system we designed to replicate the shear stress that has been measured in human capillaries, providing a minimal model of an artificial capillary. Within biological systems, proteins are subjected to considerable shear stress (ranging from force per unit area of 0.28 Pa in postcapillary venules to 9.55 Pa in the smallest diameter capillaries).³³ A maximal shear stress of 9.55 Pa is considerably higher than shear stresses which have been shown to control the aggregation of silk proteins.³⁴ The fluid flow rate throughout the diameter of the capillary varies, with the highest fluid flow rate at the middle of the capillary and a zero fluid flow rate at the capillary walls. Shear stress is maximal at the capillary walls because the force differential is maximal there. Microfluidic systems have the key advantage of being able to replicate this behavior under laminar flow conditions.³⁵ Microfluidic systems further allow transformation between space and time for precise kinetics measurements together with a convenient optical readout.³⁵ Hence, we survey the range of shear stresses and associated forces acting on biomolecules within a capillary length scale microfluidic system we designed to replicate the range of shear stresses and forces within human capillaries. Specifically, having observed increases in SASA of particular residues within our MD studies, we develop an approach to test the effects of this increased solvent accessibility on the rates of reaction of these and other residues. We observe that exclusively the residues for which SASA is increased on application of the shear-mimicking steering force experience increases in reaction rates, which shows the dependency on the level of shear applied in the capillary length scale microfluidic device.

In order to demonstrate how this finding provides a dependence of specific reaction rates on shear stress that can be used, we exploit the achieved accelerated reaction rates in a microfluidic, multidimensional cysteine biomarker assay which permits quantitative study of free and disulfide bonded cysteine residues as this relates to biomolecular size. Finally, we use our assay to monitor the structural changes catalyzed by chemical events within the heterooligomeric therapeutic antibody trastuzumab, with our results suggesting dissociation under reducing conditions such as blood plasma. We expect our portable and affordable method to find application in the study of disease biomarkers and to enable the study of biologics not prone to such dissociation within blood plasma. Furthermore, we expect our study to prompt establishment and exploration of biophysically mimetic chemistry, chemical biology, and biochemistry, in which the variety of forces utilized by nature to alter biomolecular behavior can be exploited for human purposes.

RESULTS AND DISCUSSION

High shear stresses of up to 9.55 Pa have been measured within human capillaries.³³ We questioned what impacts these may have on proteins transported through the capillary system and whether any impacts could be exploited as a biophysical tool.

Nonequilibrium MD Simulations Probe Dynamic Changes on Application of Shear-Mimicking Steering Force. To study the effect that shear stress has on the protein structure at the atomic level, we first accomplished MD simulations that mimic a simple shear flow (named Couette

flow)²⁴ on several proteins, including albumin (BSA), β -Lactoglobulin (β -Lac), β -galactosidase (BLG), and a full length IgG antibody (Tras), as shown in Figure 1 and Supporting Figs 2–5. We considered the albumin case as well suited to additional study on the effects of capillary transport because it is the most abundant serum protein, is highly conserved, is not glycosylated, and has a single conserved free cysteine residue (Cys34) which has been shown to undergo S-nitrosylation and be involved in a binding site for small molecules transported by albumin.³⁶ The positions of this residue and other disulfide bonded cysteine residues are shown in Figure 1a. We additionally include the positions of lysine residues, another type of residue prone to post-translational modifications, and intrinsically fluorescent tryptophan residues which can be indicative of changes to the structure of the aromatic protein core.³⁷

First, 0.5 μ s MD simulations of BSA protein at equilibrium, with no shear stress applied, revealed that the SASA values of lysine residues were significantly higher relative to the other residues considered (Figure 1a and Supporting Fig. 1). Subsequently, this protein was subjected to 100 ns MD simulations, in which a shear flow of 1.10×10^{-7} nm ps⁻¹ (shear stress = 9.4 Pa, Supporting Fig. 5) was applied to mimic the experimental shear stress (up to 9.55 Pa, see below). This resulted in the random diffusional motion of the protein rather than structural changes, probably due to the short simulation time.²⁴ In fact, structural fluctuations and partial unfolding of certain regions of BSA protein were observed only when the theoretical shear stress was set to 2.14×10^6 Pa (Figure 1c,d). A similar scenario was observed for the rest of the studied proteins (Supporting Figs 2–5). Under these higher shear stress conditions, we observe a 1.5-fold increase in the SASA value of Cys34 (Figure 1e). This marked increase in SASA was observed exclusively in the nonequilibrium MD simulations and not in the equilibrium (or conventional) MD simulations which were carried out using the same methods but without the introduction of the external shear flow. Moreover, we quantitatively confirmed that a free cysteine SASA increase was positively related to the shear stress (Supporting Fig. 5). An increase in SASA values was also obtained for intrinsically fluorescent Trp residues (1.4-fold) under these high shear stress conditions, while there were still no significant changes observed for Lys and disulfide bonded Cys residues. Similarly, an increase in the SASA value was observed for free Cys residues in BLG and β -Gal (Supporting Figs 2 and 3, respectively). In these cases, the MD simulations showed a lower SASA value for disulfide bonded Cys residues relative to MD simulations without a shear flow.

Alternatively, BSA, BLG, β -Gal, and a full length IgG antibody were also subjected to SMD simulations (Supporting Figs 6–12) and gave qualitatively similar results in terms of SASA values. The SMD simulations allowed us to assess a regime somewhat closer (force generally less than 200 pN for BSA, as shown in Supporting Fig. 8) to the experimental values and still observe changes within the short time scale of the SMD trajectory. Interestingly, using this technique with BSA protein, an increase in the SASA value was observed only for Cys34 residue (1.3-fold increase relative to conventional MD simulations). Although nonequilibrium molecular dynamics simulations have been used to study changes in protein structure previously, we questioned whether the increased solvent accessibility we had observed for the free cysteine residues may be able to be exploited to allow a faster reaction

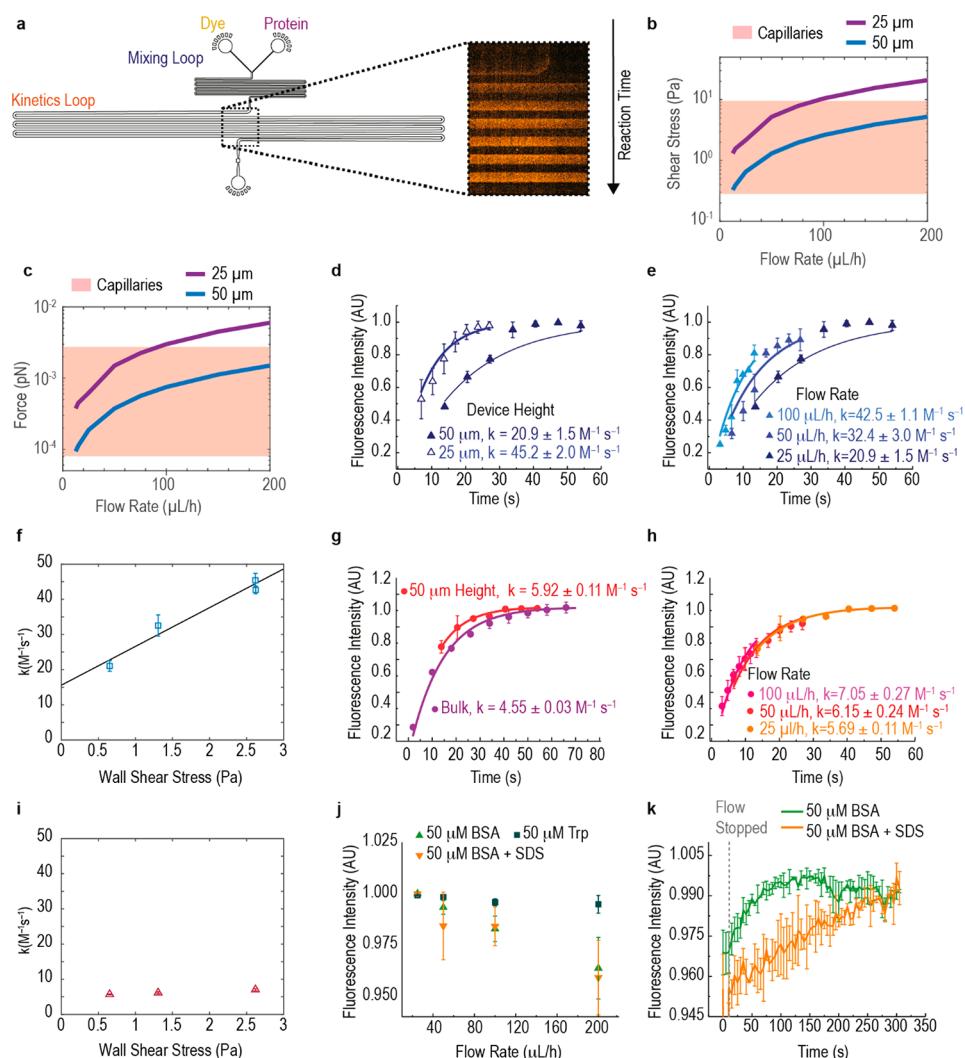


Figure 2. Biophysically mimetic shear and kinetics measurements. (a) Capillary scale kinetics device, in which optical fluorescence measurements along the kinetics loop enable calculation of the rate of reaction of protein and dye. Varying the device height and flow rate surveys the range of (b) shear stresses and (c) forces observed in human capillaries by using albumin for the force calculation. (d) Kinetics of labeling of Cys34 for 25 and 50 μm device height and (e) 25–100 $\mu\text{L}/\text{h}$ flow rate. (f) Dependence of calculated pseudo-first-order reaction rate constant on shear stress, with the linear fit rate constant = $11.1 \times \text{shear stress} + 15.4$, with $R^2 = 0.96$. (g) Kinetics of appearance of fluorescence intensity in a fluorogenic lysine labeling reaction, when moving from bulk to on-chip and (h) as a function flow rate (i) with the calculated rate constant plotted against shear stress. (j) Intrinsic tryptophan fluorescence as a function of flow rate for BSA, free Trp, and BSA + SDS. (k) Recovery of intrinsic fluorescence signal of BSA and BSA + SDS after the flow is stopped. All kinetic curves are averages of three separate experiments and standard deviation is represented by the error bars. AU = arbitrary units.

under biophysically mimetic conditions, for example, by removing a steric barrier or enhancing the nucleophilic character of the thiol group.

Reaction Rate Acceleration Dependence on Shear in Artificial Capillary Device. To test whether this increased surface accessibility results in more rapid reactivity, we performed kinetics experiments within a microfluidic device designed to provide the shear stress and forces that have been measured within capillaries. Within microfluidic systems, fluid is constrained to networks of small channels with characteristic length scales similar to biological structures.³⁸ We exploited this feature in order to design our microfluidic device (Figure 2a) to survey the range of shear stresses within capillaries³³ (0.28 to 9.55 Pa, Figure 2b) and apply corresponding levels of force (8.04×10^{-5} to 2.74×10^{-3} pN, Figure 2c) to a protein.

Cys34, for which we had observed a marked increase in SASA under shearing (Figure 1e) and shear mimicking

(Supporting Fig. 9) conditions in our simulations, is a biomarker of oxidative stress,³⁹ kidney disease, and diabetes mellitus.⁴⁰ Oxidation of Cys34 occurs based on reaction with natural disulfides and thiols without enzymatic support,⁴¹ with the Cys34 reduction state playing a key role in the binding of small molecules transported by albumin.³⁶ This allowed us to capture biologically relevant changes in the behavior of Cys34 as it is exposed to controlled shear and monitor these changes optically by trapping the reactive thiolate form with an electrophilic fluorogenic dye, 4-fluoro-7-sulfamoylbenzofuran (ABD-F).⁴² By controlling our minimal microfluidic capillary model, we were able to tune precisely the shear stress and force applied to Cys34 within the capillary range by varying the microfluidic device height and fluid flow rate. For example, as the device height decreased from 50 to 25 μm at a constant flow rate of 25 $\frac{\mu\text{L}}{\text{h}}$, shear stress increased from 0.65 to 2.16 Pa. We observed that as the device height decreases by a

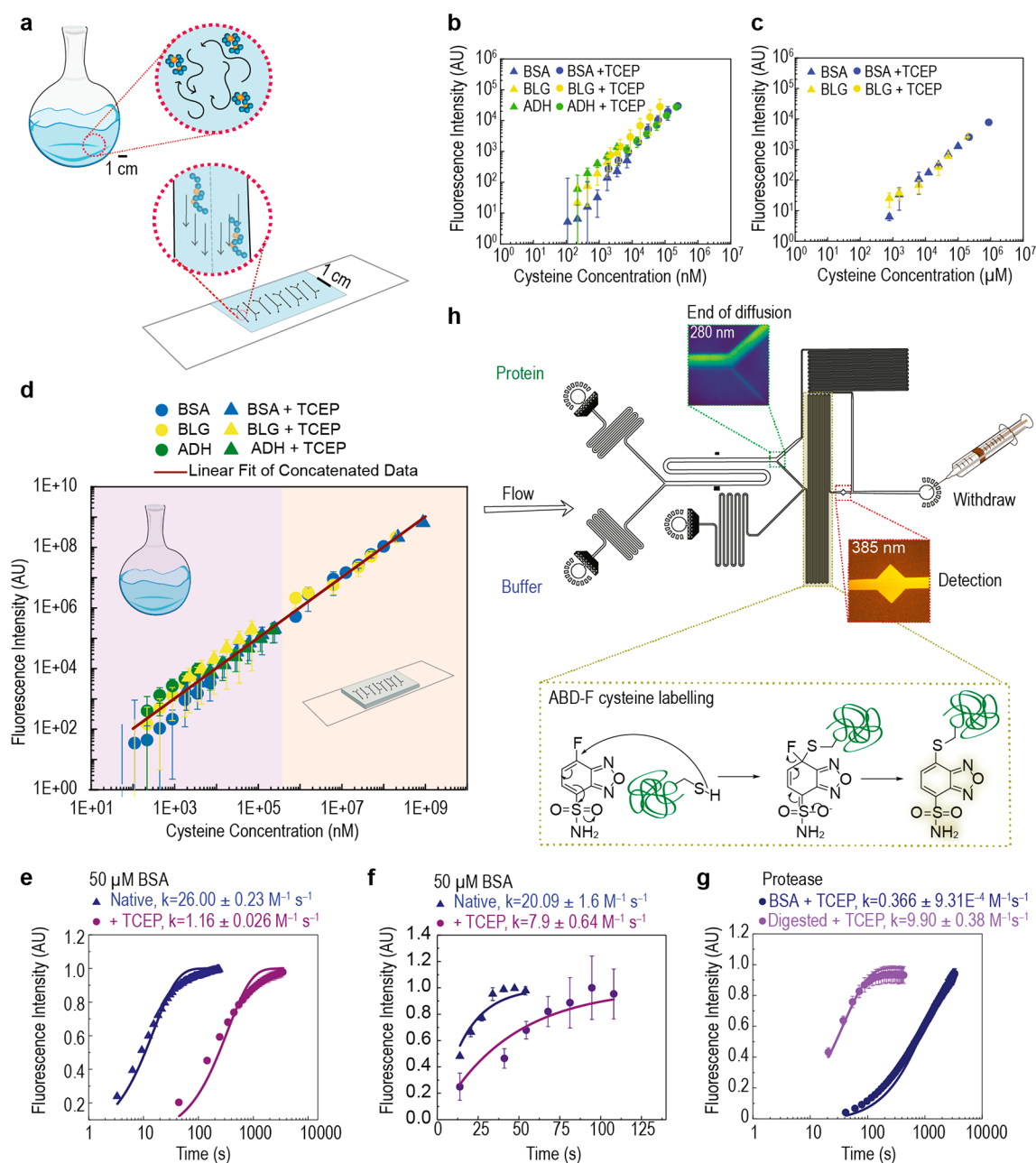


Figure 3. Development of cysteine biomarker assay. (a) Experiments are carried out in bulk or on-chip. (b) Fluorescence intensity as a function of cysteine concentration for BSA, β -lactoglobulin (βLG), and alcohol dehydrogenase (ADH) under native conditions (filled triangles) and reducing conditions with the addition of TCEP (filled circles) (b) in bulk and (c) on chip. (d) Combination of the data sets by standardizing between on-chip and in-bulk fluorescence intensity reveals a linear fit fluorescence intensity = $1.5 \times$ cysteine concentration over 7 orders of magnitude with $R^2 = 0.98$. (e) Reaction kinetics under native conditions (filled triangles) and with the addition of TCEP (filled circles) in bulk, (f) on chip, and (g) in bulk after protease digestion. (h) Microfluidic biomarker device used here and in Figure 4.

factor of 2, the rate of reaction with ABD-F increased by a factor of 2 from $20.9 \pm 1.5 \text{ M}^{-1} \text{ s}^{-1}$ to $45.2 \pm 2.0 \text{ M}^{-1} \text{ s}^{-1}$ (Figure 2d). Interestingly, previous results⁴³ had reported that this residue is reactive only when the protein is subjected to shear stress. However, we observed reactivity in the absence of flow, which could be expected since the previous study used a large fluorophore with three negative charges. Thus, the steric crowding and electrostatic effects of labeling a buried cysteine residue in this way are likely responsible for the observed lack of reactivity of Cys34. In contrast, our fluorophore was significantly smaller and had a lower net charge, which could favor labeling of the free cysteine in the absence of flow.

To quantify the reaction rate changes we had observed (Figure 2d,e), we plotted the reaction rate as a function of shear stress (Figure 2f). Satisfyingly, we observe a linear relationship (reaction rate $\left(\frac{1}{\text{M} \times \text{s}}\right) = 11.1 \frac{\text{s}}{\text{kg} \times \text{M} \times \text{m}}$ shear stress $\left(\frac{\text{N}}{\text{m}^2}\right) + 15.41 \frac{1}{\text{M} \times \text{s}}$, $R^2 = 0.96$), which indicated that shear stress applied within our capillary scale microfluidic kinetics device drove the measured increase in reaction rate.

As a control, we also examined any changes in reaction rates that occurred for residues for which we had not observed a significant increase in solvent accessibility on application of the

shear-mimicking steering force in our MD simulations. To achieve this, we modified lysine residues with fluorogenic ortho-phthalaldehyde (OPA)^{44,45} and monitored the effects of applying the same levels of shear on the kinetics of the labeling reaction (Figure 2g,h). Notably, shear stress did not significantly affect the reaction rate for lysine residues (Figure 2i).

To further assess a possible conformational change affecting Cys34 but not lysine residues, we examined aromatic residue exposure by measuring the intrinsic fluorescence intensity of tryptophan residues; this is solvatochromic with the tryptophan local environment with fluorescence decreases associated with a decrease in structure.⁴⁶

An increase in flow rate to 200 $\mu\text{L}/\text{h}$ decreased tryptophan FI by 4% (Figure 2j) which was reversible after the flow was stopped (Figure 2k). The fact that the small change was just detectable over error was consistent with no large scale structural changes observed in the MD simulation studies under shear stress conditions (Figure 1d) as well as the lack of significant SASA increase for tryptophan residues on application of the steering force (Supporting Fig. 8). No change was observed for free tryptophan in solution (Figure 2j).

Collectively, our results (Figures 1 and 2) suggest that the force acting on a protein from the shear stress caused by capillary transport does not induce large scale structural or unfolding changes, as has been observed, for example, in amyloid proteins.^{34,47} Instead, the shearing force acting on key reactive residues normally buried within the protein structure promotes local structural changes that increase the solvent accessibility of these residues, causing them to react more quickly. This hypothesis would elucidate the mechanism by which shear stress has been observed to activate signaling pathways, such as the MAPK, JNK, and ERK pathways⁴⁸ as well as suggesting that organisms can use transport through their vascular system to modulate protein behavior through post-translational modifications. Interestingly, transport through the gated capillary network is under hormonal control,⁴⁹ lending further support to the idea of shear-mediated post-translational modification modulation in response to stimuli such as stress.

Utilizing Rapid Artificial Capillary Reaction Rate in a Microfluidic Multidimensional Cysteine Biomarker Tool. Our results suggested that biophysically mimetic systems may unlock higher reaction rates. As an application, we developed a multidimensional assay for cysteine biomarkers that incorporates biomarker size and cysteine reduction state across native and reducing conditions in a highly portable microfluidic format.

To do this, we first establish a linear relationship between free cysteine concentration (cysteine residues which are not disulfide bonded) and fluorescence intensity (FI) of ABD-F labeled cysteine both *on chip* (Figure 3b, filled triangles) and *in bulk* (Figure 3c, filled triangles). Schematics of the on chip and in bulk reactions are shown in Figure 3a. Disulfide bonded cysteine residues are also attractive targets because they are involved in neurodegenerative diseases, immune response, vascular inflammation, and cancer aggressiveness.^{50,51} However, fluorogenically labeling these residues is challenging because it requires liberating the thiol nucleophile without the nucleophilic reducing agent itself reacting with the electrophilic fluorogenic dye. We observed that *in situ* reduction of cysteine disulfide bonds with Tris (2-carboxyethyl) phosphine

(TCEP) prior to reaction with ABD-F did not generate significant background fluorescence, and the reactions in bulk (Figure 3b, filled circles) and on chip (Figure 3c, filled circles) both proceeded quantitatively.

Combining our data sets (Figure 3b,c) reveals that our approach is quantitative across 7 orders of magnitude in concentration (Figure 3d). Data, from both free and disulfide-bonded cysteine and both on chip and bulk assay formats across all proteins studied, all fit a single line with a high correlation coefficient ($R^2 = 0.98$). We performed an unconstrained linear fit to the double logarithm of the data and obtained the equation $\log y = 1.006 \log x + 0.019$; this results in the linear equation $y = 1.05x$ with no power dependence, which indicates exceptional linearity and complete conversion across free and disulfide bonded cysteine residues and across in bulk and on chip assay formats (Figure 3d). However, addition of TCEP retarded the labeling reaction both in bulk (Figure 3e) and on chip (Figure 3f). The reaction rate on chip ($7.9 \pm 0.64 \text{ M}^{-1} \text{ s}^{-1}$) was comparable to the reaction rate when a protease was added to the bulk reaction in Figure 3g ($9.9 \pm 0.38 \text{ M}^{-1} \text{ s}^{-1}$). Increased solvent accessibility, achieved by either microfluidic shear stress or protease digestion, mitigated the reaction retardation effect, which permitted rapid labeling of cysteine residues on a microfluidic chip in real time, and enabled this on chip labeling to form part of a larger on chip measurement strategy.

We note that although there are existing approaches for the labeling of cysteine biomarkers,^{52,53} these generally require the use of pre-labeled proteins. Beneficially, the fluorogenic (fluorescence generating) feature of our approach means that protein pre-labeling is not required, and accordingly there is no need to purify protein from unreacted dye. Moreover, any potential impact of the presence of the label on the protein behavior under observation can be eliminated when particular on-chip labeling and analysis strategies are applied. The rapid reaction kinetics and observed quantitative nature of the labeling reaction (Figures 1d–f and 3e,f) permitted us to achieve specifically a latent analysis approach⁴⁵ for native microfluidic diffusional sizing in which measurement of a labeled protein revealed the protein hydrodynamic radius (R_{H}) before it was labeled on chip.⁴⁵

Our cysteine biomarker chip design is shown in Figure 3h. Streams of protein and buffer flowed adjacent to one another within the diffusion channel; mass transport of protein across the diffusion channel was entirely due to diffusion which is directly related to protein size (R_{H}).³⁵ Smaller species diffused further than larger species, and the detected fluorescence intensity was ultimately related to protein size in comparison to simulation (Supporting Fig. 17). Protein that had diffused across the diffusion channel was labeled via ABD-F reaction at cysteine residues, with or without the addition of TCEP and in a buffered solution. Within the labeling loop, proteins were exposed to shear within the capillary range explored here (Figure 2b) of 0.44 Pa permitting rapid reaction within the on chip labeling module. Because both protein size in a native and reducing environment are available, our approach enables a novel nondisruptive assessment of the structural effect of protein disulfide bond cleavage.

We validate our assay by measuring proteins and protein complexes that vary in molecular weight, structure, and oligomeric state including dimeric BLG, monomeric BSA, tetrameric alcohol dehydrogenase (ADH), and tetrameric β -galactosidase (β -Gal) (Figure 4a). We observe R_{H} , predicted

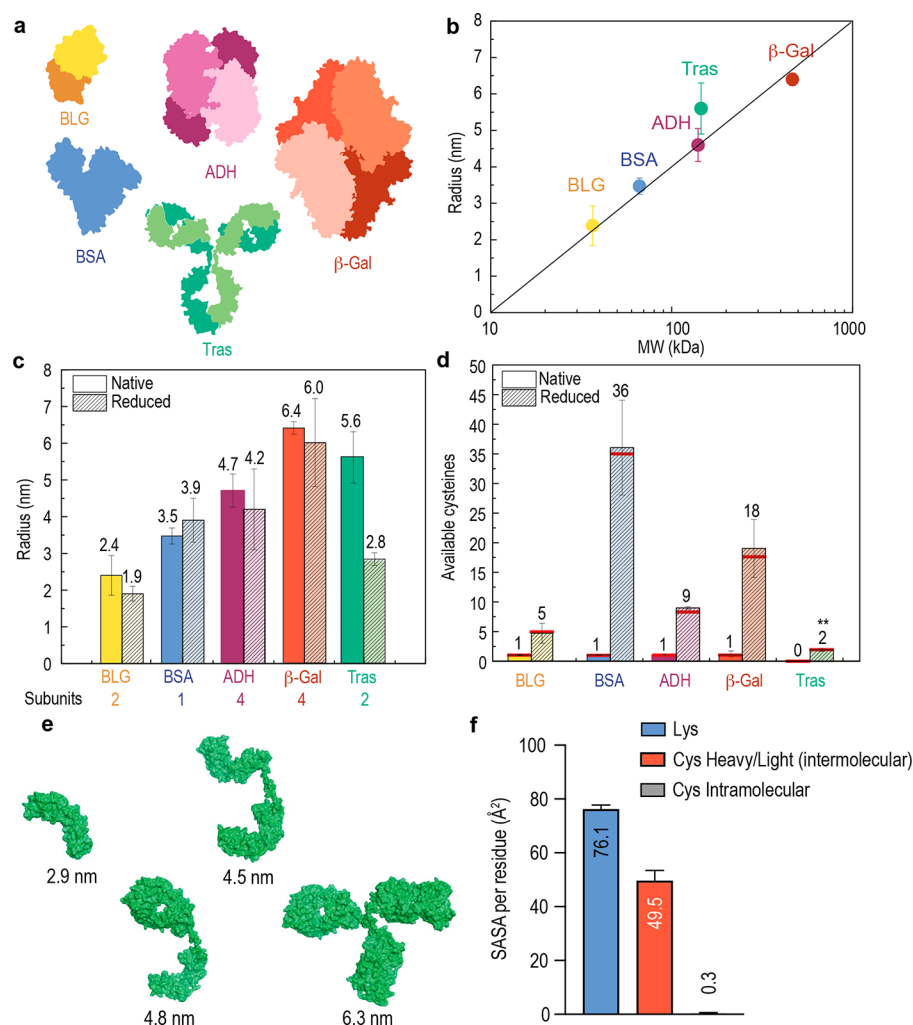


Figure 4. Correlation of chemical and physical structural changes. (a) Crystal structures of the proteins and protein complexes used including β -lactoglobulin (BLG), ADH, β -Gal, BSA, and Tras, with protein chains indicated colorimetrically. (b) Measured protein and protein complex hydrodynamic radius as a function of molecular weight under native conditions. (c) Measured hydrodynamic radius for each protein and protein complex under native and reducing conditions. (d) Absolute number of available cysteine residues measured under native and reducing conditions. (e) Simulated Tras fragment sizes with no dissociation, half antibody dissociation, or half antibody and heavy and light chain dissociation. (f) Average SASA values of different residues of Tras derived from 100 ns MD simulations with shear stress (8.54×10^5 Pa).

by scaling laws⁵⁴ for all globular proteins (Figure 4b) in a native environment. R_H values are comparable within error in a reducing environment, suggesting that significant global structural changes have not taken place. Because labeling is quantitative, when the protein concentration is known the fluorescence intensity depends exclusively on the number of total or free cysteine residues within the protein. We calculate the absolute number of cysteine residues for each protein and protein complex detected under native and reducing conditions and compare with expected values (Figure 4d). All of our results match expected numbers of available cysteines within error.

Therapeutic Antibody Dissociation in Blood-Plasma-like Reducing Environment. Finally, having validated our assay, we applied it to probe the behavior of a biologically relevant system. Trastuzumab is a humanized IgG monoclonal antibody used in the treatment of human epidermal growth factor receptor 2 (HER2) positive breast⁵⁵ and stomach⁵⁶ cancers. Trastuzumab binds to the extracellular domain of HER2, promoting internalization and downregulation of HER2 mediated cell division.⁵⁷ When trastuzumab is administered via

intravenous injection, it passes through capillaries and is in a reducing environment (blood plasma).⁵⁸ We applied our assay in order to quantify any structural changes that may occur when trastuzumab is placed in a reducing environment and confined to the capillary length scale.

In a nonreducing environment, we measured an R_H for trastuzumab which exceeds by about 25% the R_H predicted for globular proteins, as we expected given its extended conformation. However, interestingly when trastuzumab was placed in a reducing environment, it is measured R_H decreases from 5.0 ± 0.6 nm to 2.8 ± 0.2 nm, suggesting a dissociation event. When trastuzumab was placed in a reducing environment, the measured absolute number of available cysteines increased from 0 to 2. This suggested that only cysteine residues within interchain disulfide bonds are being reduced and labeled, and reduction of these disulfide bonds was consistent with the apparent dissociation event.

We modeled the trastuzumab antibody, the trastuzumab half antibody, and the heavy and light chain fragments of the trastuzumab half antibody (Figure 4e). While dissociation of a hetero-oligomer like trastuzumab by definition creates a

mixture of different monomers, our diffusional assay preferentially separates, labels, and detects the smaller species which have diffused into the labeling region (Supporting Fig. 16). The R_H we measured for trastuzumab under reducing conditions, 2.8 ± 0.2 nm, was in agreement with the size modeled for trastuzumab light chain fragments (2.9 nm), suggesting trastuzumab dissociation into both half antibody and heavy and light chain fragments. MD simulations of Tras carried out with a shear flow (or alternatively, SMD simulations) showed that the intermolecular disulfide bridges (heavy and light chain) had a significantly higher SASA upon application of shear stress than the intramolecular disulfides (Supporting Figs 4 and 12), supporting the idea that these particular disulfide bonds would have been highly accessible to the TCEP reducing agent when shear stress was applied in the microfluidic device. Finally, we performed native mass spectrometry experiments to directly measure the stoichiometry under reducing, shearing conditions as in our microfluidic device and in capillaries (Supporting Fig. 18b). Satisfyingly, we observed dissociation of the monoclonal antibody into heavy and light chain fragments in reducing, shearing conditions, as our experiments and simulations indicated, which was not observed in our control experiments under nonreducing conditions (Supporting Fig. 18a).

CONCLUSION

Heavy/light chain dissociation within a reducing environment, such as blood plasma, reduces the affinity of trastuzumab and other monoclonal antibodies.⁵⁹ Our experimental and simulation results, which we confirmed via native mass spectrometry, suggest that trastuzumab may be dissociated into heavy and light chain components in plasma, potentially reducing its affinity. Further studies should use our assay to study dissociation of trastuzumab in plasma. Our results also suggest that *in vivo* fluorescence techniques, for example, involving FRET, should be used to assess the structural integrity of trasutzumab that has been transported through capillaries in blood plasma. Finally, our assay can be used to screen and identify variants of trasutzumab and other monoclonal antibodies which do not dissociate in a reducing environment and which may retain higher affinity in plasma. This may be achieved by substituting heavy chains that form disulfide bonds with higher reduction potentials. Our assay could also be used in the study of other biologics or disease associated cysteine biomarkers.

Our results further suggest that shear stress experienced within microfluidic devices may modulate protein structure and that reaction rates for some reactions may be accelerated relative to their bulk counterparts. The research area of nanofluidics could enable particularly rapid reactivity due to the particularly small channel characteristic length scales and associated high shear rates, albeit with potential structural changes.

More broadly, we have provided a proof-of-concept demonstration of the potential of biophysically mimetic chemistry. We anticipate that mirroring nature and its use of its physical architecture to modulate protein function will find broad application in chemistry, biochemistry, chemical biology, and biotechnology.

ASSOCIATED CONTENT

Supporting Information

The Supporting Information is available free of charge at <https://pubs.acs.org/doi/10.1021/jacs.1c03681>.

Materials, detailed methods, supporting figures, table, and references (PDF)

AUTHOR INFORMATION

Corresponding Authors

Francisco Corzana – Departamento de Química, Centro de Investigación en Síntesis Química, Universidad de La Rioja, 26006 Logroño, Spain; orcid.org/0000-0001-5597-8127; Email: francisco.corzana@unirioja.es

Tuomas P. J. Knowles – Yusuf Hamied Department of Chemistry, University of Cambridge, Cambridge CB2 1EW, United Kingdom; Cavendish Laboratory, University of Cambridge, CB3 0HE Cambridge, United Kingdom; orcid.org/0000-0002-7879-0140; Email: tpjk2@cam.ac.uk

Gonçalo J. L. Bernardes – Yusuf Hamied Department of Chemistry, University of Cambridge, Cambridge CB2 1EW, United Kingdom; Instituto de Medicina Molecular João Lobo Antunes, Faculdade de Medicina de Universidade de Lisboa, 1649-028 Lisboa, Portugal; orcid.org/0000-0001-6594-8917; Email: gb453@cam.ac.uk

Authors

Tuuli A. Hakala – Yusuf Hamied Department of Chemistry, University of Cambridge, Cambridge CB2 1EW, United Kingdom; orcid.org/0000-0002-2075-3451

Emma V. Yates – Yusuf Hamied Department of Chemistry, University of Cambridge, Cambridge CB2 1EW, United Kingdom

Pavan K. Challa – Yusuf Hamied Department of Chemistry, University of Cambridge, Cambridge CB2 1EW, United Kingdom; orcid.org/0000-0002-0863-381X

Zenon Toprakcioglu – Yusuf Hamied Department of Chemistry, University of Cambridge, Cambridge CB2 1EW, United Kingdom; orcid.org/0000-0003-1964-8432

Karthik Nadendla – Yusuf Hamied Department of Chemistry, University of Cambridge, Cambridge CB2 1EW, United Kingdom

Dijana Matak-Vinkovic – Yusuf Hamied Department of Chemistry, University of Cambridge, Cambridge CB2 1EW, United Kingdom

*Christopher M. Dobson – Yusuf Hamied Department of Chemistry, University of Cambridge, Cambridge CB2 1EW, United Kingdom

Rodrigo Martínez – Departamento de Química, Universidad de La Rioja, 26006 Logroño, Spain; orcid.org/0000-0002-5850-8494

Complete contact information is available at: <https://pubs.acs.org/doi/10.1021/jacs.1c03681>

Author Contributions

*T.A.H. and E.V.Y. contributed equally to the work presented.

Notes

The authors declare no competing financial interest.

#Since contributing to the work presented in this article, sadly, Professor Christopher M. Dobson has passed away (September 8, 2019). The authors are very grateful for his contribution to this work.

ACKNOWLEDGMENTS

This project has received funding from the European Union's Horizon 2020 research and innovation programme under Grant Agreement No. 852985 and Marie Skłodowska-Curie Grant Agreement No. 67500. We also thank the European Research Council (ERC Grant PhysProt G.A. No. 337969 to T.P.J.K.), Emmanuel College (E.V.Y.), Royal Society (Grant URF80019 to G.J.L.B.), FCT Portugal (Stimulus Grant CEECIND/00453/2018 to G.J.L.B.), *Agencia Estatal Investigación* of Spain (AEI, Grant RTI2018-099592-B-C21 to F.C. and Grant PGC2018-098561-B-C21 to R.M.), the BBSRC (T.P.J.K.), the Newman Foundation (T.P.J.K.), the Wellcome Trust (T.P.J.K.), and the Cambridge Centre for Misfolding Diseases for funding support. The authors thank Dr. Vikki Cantrill for her help with the editing of this manuscript.

REFERENCES

- (1) Davis, B. G. Mimicking Posttranslational Modifications of Proteins. *Science* **2004**, *303* (5657), 480–481.
- (2) Low, L. A.; Mummery, C.; Berridge, B. R.; Austin, C. P.; Tagle, D. A. Organs-on-chips: into the next decade. *Nat. Rev. Drug Discovery* **2021**, *20*, 345–361.
- (3) Levin, A.; Hakala, T. A.; Schnaider, L.; Bernardes, G. J. L.; Gazit, E.; Knowles, T. P. J. Biomimetic peptide self-assembly for functional materials. *Nat. Rev. Chem.* **2020**, *4*, 615–634.
- (4) Hoyt, E. A.; Cal, P. M. S. D.; Oliveira, B. L.; Bernardes, G. J. L. Contemporary approaches to site-selective protein modification. *Nat. Rev. Chem.* **2019**, *3*, 147–171.
- (5) Godfrey, R. C.; Green, N. J.; Nichol, G. S.; Lawrence, A. L. Total synthesis of breviramide A. *Nat. Chem.* **2020**, *12*, 615–619.
- (6) Gilmore, J. M.; Scheck, R. A.; Esser-Kahn, A. P.; Joshi, N. S.; Francis, M. B. N-Terminal Protein Modification through a Biomimetic Transamination Reaction. *Angew. Chem., Int. Ed.* **2006**, *45*, 5307–5311.
- (7) Zhu, A.; Li, X.; Bai, L.; Zhu, G.; Guo, Y.; Lin, J.; Cui, Y.; Tian, G.; Zhang, L.; Wang, J.; Li, X. D.; Li, L. Biomimetic α -selective ribosylation enables two-step modular synthesis of biologically important ADP-ribosylated peptides. *Nat. Commun.* **2020**, *11*, 5600.
- (8) Chen, L.; Quan, H.; Xu, Z.; Wang, H.; Xia, Y.; Lou, L.; Yang, W. A modular biomimetic strategy for the synthesis of macrolide P-glycoprotein inhibitors via Rh-catalyzed C-H activation. *Nat. Commun.* **2020**, *11*, 2151.
- (9) Park, S. Y.; Hwang, I.-S.; Lee, H.-J.; Song, C. E. Biomimetic catalytic transformation of toxic α -oxoaldehydes to high-value chiral α -hydroxythioesters using artificial glyoxalase I. *Nat. Commun.* **2017**, *8*, 14877.
- (10) White, D. A.; Buell, A. K.; Knowles, T. P.; Welland, M. E.; Dobson, C. M. Protein aggregation in crowded environments. *J. Am. Chem. Soc.* **2010**, *132*, 5170–5175.
- (11) Sukenik, S.; Politi, R.; Ziserman, L.; Danino, D.; Friedler, A.; Harries, D. Crowding alone cannot account for cosolute effect on amyloid aggregation. *PLoS One* **2011**, *6*, No. e15608.
- (12) Engler, A. J.; Sen, S.; Sweeney, H. L.; Discher, D. E. Matrix elasticity directs stem cell lineage specification. *Cell* **2006**, *126*, 677–689.
- (13) Petrie, R. J.; Yamada, K. M. Fibroblasts Lead the Way: A Unified View of 3D Cell Motility. *Trends Cell Biol.* **2015**, *25*, 666–674.
- (14) Tzima, E.; Irani-Tehrani, M.; Kiesses, W. B.; Dejana, E.; Schultz, D. A.; Engelhardt, B.; Cao, G.; DeLisser, H.; Schwartz, M. A. A mechanosensory complex that mediates the endothelial cell response to fluid shear stress. *Nature* **2005**, *437*, 426–431.
- (15) Chatzizisis, Y. S.; Coskun, A. U.; Jonas, M.; Edelman, E. R.; Feldman, C. L.; Stone, P. H. Role of endothelial shear stress in the natural history of coronary atherosclerosis and vascular remodeling: molecular, cellular, and vascular behavior. *J. Am. Coll. Cardiol.* **2007**, *49*, 2379–2393.
- (16) Huang, B.; Chen, S. C.; Wang, D. L. Shear flow increases S-nitrosylation of proteins in endothelial cells. *Cardiovasc. Res.* **2009**, *83*, 536–546.
- (17) Bekard, I. B.; Asimakis, P.; Bertolini, J.; Dunstan, D. E. The effects of shear flow on protein structure and function. *Biopolymers* **2011**, *95*, 733–745.
- (18) Sterpone, F.; Derreumaux, P.; Melchionna, S. Molecular Mechanism of Protein Unfolding under Shear: A Lattice Boltzmann Molecular Dynamics Study. *J. Phys. Chem. B* **2018**, *122*, 1573–1579.
- (19) Sterpone, F.; Derreumaux, P.; Melchionna, S. Protein Simulations in Fluids: Coupling the OPEP Coarse-Grained Force Field with Hydrodynamics. *J. Chem. Theory Comput.* **2015**, *11*, 1843–1853.
- (20) Lemak, A. S.; Lepock, J. R.; Chen, J. Z. Y. Molecular dynamics simulations of a protein model in uniform and elongational flows. *Proteins: Struct., Funct., Genet.* **2003**, *51*, 224–235.
- (21) Szymczak, P.; Cieplak, M. Proteins in a shear flow. *J. Chem. Phys.* **2007**, *127*, 155106.
- (22) Szymczak, P.; Cieplak, M. Influence of hydrodynamic interactions on mechanical unfolding of proteins. *J. Phys.: Condens. Matter* **2007**, *19*, 285224.
- (23) Chiricotto, M.; Melchionna, S.; Derreumaux, P.; Sterpone, F. Hydrodynamic effects on β -amyloid (16–22) peptide aggregation. *J. Chem. Phys.* **2016**, *145*, 035102.
- (24) Walinda, E.; Morimoto, D.; Shirakawa, M.; Scheler, U.; Sugase, K. Visualizing protein motion in Couette flow by all-atom molecular dynamics. *Biochim. Biophys. Acta, Gen. Subj.* **2020**, *1864*, 129383.
- (25) Izrailev, S.; Stepaniants, S.; Isralewitz, B.; Kosztin, D.; Lu, H.; Molnar, F.; Wrigger, W.; Schulten, K. Steered Molecular Dynamics. In *Computational Molecular Dynamics: Challenges, Methods, Ideas*; Deuffhard, P., Hermans, J., Leimkuhler, B., Mark, A. E., Reich, S., Skeel, R. D., Eds.; Springer Berlin Heidelberg: Berlin, Heidelberg, Germany, 1999; pp 39–65.
- (26) Park, S.; Schulten, K. Calculating potentials of mean force from steered molecular dynamics simulations. *J. Chem. Phys.* **2004**, *120*, 5946–5961.
- (27) Jorgensen, W. L. Pulled from a protein's embrace. *Nature* **2010**, *466*, 42–43.
- (28) Grubm ller, H.; Heymann, B.; Tavan, P. Ligand Binding: Molecular Mechanics Calculation of the Streptavidin-Biotin Rupture Force. *Science* **1996**, *271*, 997–999.
- (29) Ndlovu, H.; Ashcroft, A. E.; Radford, S. E.; Harris, S. A. Effect of sequence variation on the mechanical response of amyloid fibrils probed by steered molecular dynamics simulation. *Biophys. J.* **2012**, *102*, 587–596.
- (30) Kang, Y.; Lü, S.; Ren, P.; Huo, B.; Long, M. Molecular dynamics simulation of shear- and stretch-induced dissociation of P-selectin/PSGL-1 complex. *Biophys. J.* **2012**, *102*, 112–120.
- (31) Xiao, B.-L.; Ning, Y.-N.; Niu, N.-N.; Li, D.; Moosavi-Movahedi, A. A.; Sheibani, N.; Hong, J. Steered molecular dynamic simulations of conformational lock of Cu, Zn-superoxide dismutase. *Sci. Rep.* **2019**, *9*, 4353.
- (32) Ho, B. K.; Agard, D. A. An improved strategy for generating forces in steered molecular dynamics: the mechanical unfolding of titin, e2lip3 and ubiquitin. *PLoS One* **2010**, *5*, No. e13068.
- (33) Koutsiaris, A. G.; Tachmitzi, S. V.; Batis, N.; Kotoula, M. G.; Karabatsas, C. H.; Tsironi, E.; Chatzoulis, D. Z. Volume flow and wall shear stress quantification in the human conjunctival capillaries and post-capillary venules in vivo. *Biorheology* **2007**, *44*, 375–386.
- (34) Toprakcioglu, Z.; Knowles, T. P. J. Shear-mediated sol-gel transition of regenerated silk allows the formation of Janus-like microgels. *Sci. Rep.* **2021**, *11*, 6673.
- (35) Squires, T. M.; Quake, S. R. Microfluidics: Fluid physics at the nanoliter scale. *Rev. Mod. Phys.* **2005**, *77*, 977.
- (36) Stewart, A. J.; Blindauer, C. A.; Berezenko, S.; Sleep, D.; Tooth, D.; Sadler, P. J. Role of Tyr84 in controlling the reactivity of Cys34 of human albumin. *FEBS J.* **2005**, *272*, 353–362.
- (37) Vivian, J. T.; Callis, P. R. Mechanisms of tryptophan fluorescence shifts in proteins. *Biophys. J.* **2001**, *80*, 2093–2109.

- (38) Whitesides, G. M. The origins and the future of microfluidics. *Nature* **2006**, *442*, 368–373.
- (39) Lim, Z. X.; Duong, M. N.; Boyatzis, A. E.; Golden, E.; Vrieling, A.; Fournier, P. A.; Arthur, P. G. Oxidation of cysteine 34 of plasma albumin as a biomarker of oxidative stress. *Free Radical Res.* **2020**, *54*, 91–103.
- (40) Nagumo, K.; Tanaka, M.; Chuang, V. T. G.; Setoyama, H.; Watanabe, H.; Yamada, N.; Kubota, K.; Tanaka, M.; Matsushita, K.; Yoshida, A.; Jinnouchi, H.; Anraku, M.; Kadowaki, D.; Ishima, Y.; Sasaki, Y.; Otagiri, M.; Maruyama, T. Cys34-Cysteinylated Human Serum Albumin Is a Sensitive Plasma Marker in Oxidative Stress-Related Chronic Diseases. *PLoS One* **2014**, *9*, No. e85216.
- (41) Bocedi, A.; Cattani, G.; Stella, L.; Massoud, R.; Ricci, G. Thiol disulfide exchange reactions in human serum albumin: the apparent paradox of the redox transitions of Cys34. *FEBS J.* **2018**, *285*, 3225–3237.
- (42) Imai, K.; Uzu, S.; Toyo'oka, T. Fluorogenic reagents, having benzofurazan structure, in liquid chromatography. *J. Pharm. Biomed. Anal.* **1989**, *7*, 1395–1403.
- (43) Dobson, J.; Kumar, A.; Willis, L. F.; Tuma, R.; Higazi, D. R.; Turner, R.; Lowe, D. C.; Ashcroft, A. E.; Radford, S. E.; Kapur, N.; Brockwell, D. J. Inducing protein aggregation by extensional flow. *Proc. Natl. Acad. Sci. U. S. A.* **2017**, *114* (18), 4673–4678.
- (44) Roth, M. Fluorescence reaction for amino acids. *Anal. Chem.* **1971**, *43*, 880–882.
- (45) Yates, E. V.; Müller, T.; Rajah, L.; De Genst, E. J.; Arosio, P.; Linse, S.; Vendruscolo, M.; Dobson, C. M.; Knowles, T. P. J. Latent analysis of unmodified biomolecules and their complexes in solution with attomole detection sensitivity. *Nat. Chem.* **2015**, *7*, 802–809.
- (46) Toprakcioglu, Z.; Challa, P.; Xu, C.; Knowles, T. P. J. Label-Free Analysis of Protein Aggregation and Phase Behavior. *ACS Nano* **2019**, *13*, 13940–13948.
- (47) Peng, Q.; Zhang, Y.; Lu, L.; Shao, H.; Qin, K.; Hu, X.; Xia, X. Recombinant spider silk from aqueous solutions via a bio-inspired microfluidic chip. *Sci. Rep.* **2016**, *6*, 36473.
- (48) Jalali, S.; Li, Y.-S.; Sotoudeh, M.; Yuan, S.; Li, S.; Chien, S.; Shyy, J. Y.-J. Shear Stress Activates p60src-Ras-MAPK Signaling Pathways in Vascular Endothelial Cells. *Arterioscler., Thromb., Vasc. Biol.* **1998**, *18*, 227–234.
- (49) Schaeffer, M.; Hodson, D. J.; Lafont, C.; Mollard, P. Endocrine cells and blood vessels work in tandem to generate hormone pulses. *J. Mol. Endocrinol.* **2011**, *47*, R59–66.
- (50) Fass, D. Disulfide Bonding in Protein Biophysics. *Annu. Rev. Biophys.* **2012**, *41*, 63–79.
- (51) Mossuto, M. F. Disulfide Bonding in Neurodegenerative Misfolding Diseases. *Int. J. Cell Biol.* **2013**, *2013*, 318319.
- (52) Bernardim, B.; Cal, P. M. S. D.; Matos, M. J.; Oliveira, B. L.; Martínez-Sáez, N.; Albuquerque, I. S.; Perkins, E.; Corzana, F.; Burtoloso, A. C. B.; Jiménez-Osés, G.; Bernardes, G. J. L. Stoichiometric and irreversible cysteine-selective protein modification using carbonylacrylic reagents. *Nat. Commun.* **2016**, *7*, 13128.
- (53) Ochtrop, P.; Hackenberger, C. P. R. Recent advances of thiol-selective bioconjugation reactions. *Curr. Opin. Chem. Biol.* **2020**, *58*, 28–36.
- (54) Tomasso, M. E.; Tarver, M. J.; Devarajan, D.; Whitten, S. T. Hydrodynamic Radii of Intrinsically Disordered Proteins Determined from Experimental Polyproline II Propensities. *PLoS Comput. Biol.* **2016**, *12*, No. e1004686.
- (55) Emens, L. A.; Davidson, N. E. Trastuzumab in breast cancer. *Oncology (Williston Park)* **2004**, *18* (9), 1117–1128.
- (56) Gunturu, K. S.; Woo, Y.; Beaubier, N.; Remotti, H. E.; Saif, M. W. Gastric cancer and trastuzumab: first biologic therapy in gastric cancer. *Ther. Adv. Med. Oncol.* **2013**, *5*, 143–151.
- (57) Vu, T.; Claret, F. X. Trastuzumab: updated mechanisms of action and resistance in breast cancer. *Front. Oncol.* **2012**, *2*, 62.
- (58) Schafer, F. Q.; Buettner, G. R., Redox State and Redox Environment in Biology. In *Signal Transduction by Reactive Oxygen and Nitrogen Species: Pathways and Chemical Principles*; Forman, H. J., Fukuto, J., Torres, M., Eds.; Springer Netherlands: Dordrecht, The Netherlands, 2003; pp 1–14.
- (59) Farràs, M.; Román, R.; Camps, M.; Miret, J.; Martínez, Ó.; Pujol, X.; Casablancas, A.; Cairó, J. J. Heavy chain dimers stabilized by disulfide bonds are required to promote in vitro assembly of trastuzumab. *BMC Mol. Cell Biol.* **2020**, *21*, 2.